REPORT DOCUMENTATION PAGE

Form Approved OMB NO. 0704-0188

1. REPORT DATE (DD-MM-YYYY)	2. REPORT TYPE	3. DATES COVERED (From - To)
21-07-2015	Final Report	7-Jul-2014 - 6-Apr-2015

4. TITLE AND SUBTITLE

Final Report: Growth of Large-Area, Free-Standing, Ultrathin 2D Nanomaterials at Solution Interface

5a. CONTRACT NUMBER
W911NF-14-1-0325

5b. GRANT NUMBER

5c. PROGRAM ELEMENT NUMBER
611102

6. AUTHORS
Xudong Wang, Fei Wang

5d. PROJECT NUMBER

5e. TASK NUMBER

5f. WORK UNIT NUMBER

7. PERFORMING ORGANIZATION NAMES AND ADDRESSES
University of Wisconsin - Madison 1.00
Suite 6401
21 N Park St
Madison, WI 53715 -1218

8. PERFORMING ORGANIZATION REPORT NUMBER

9. SPONSORING/MONITORING AGENCY NAME(S) AND ADDRESS (ES)
U.S. Army Research Office
P.O. Box 12211
Research Triangle Park, NC 27709-2211

10. SPONSOR/MONITOR'S ACRONYM(S)
ARO

11. SPONSOR/MONITOR'S REPORT NUMBER(S)
65630-MS-II.2

12. DISTRIBUTION AVAILIBILITY STATEMENT
Approved for Public Release; Distribution Unlimited

13. SUPPLEMENTARY NOTES
The views, opinions and/or findings contained in this report are those of the author(s) and should not contrued as an official Department of the Army position, policy or decision, unless so designated by other documentation.

14. ABSTRACT
The development of large and ultrathin nanosheets has been focused on naturally layered materials – the van der Waals solids, such as graphene and transition metal dichalcogenides. Bottom-up synthesis of nanosheets of non-layered materials has been unsatisfactory and limited success has been achieved on nanosheets with sizes below a few hundred nanometers. In this project, We demonstrated that surfactant monolayers could serve as a floating template supporting the nucleation and growth of 2D nanomaterials in large area beyond the limitation of van der Waals solids. Through this approach, 2 to 3 nm thick, monocrystalline ZnO nanosheets with sizes up to tens of

15. SUBJECT TERMS
zinc oxide nanosheets, water-air interface, surfactant monolayer, epitaxial growth

16. SECURITY CLASSIFICATION OF:			17. LIMITATION OF ABSTRACT	15. NUMBER OF PAGES	19a. NAME OF RESPONSIBLE PERSON
a. REPORT	b. ABSTRACT	c. THIS PAGE			XUDONG WANG
UU	UU	UU	UU		19b. TELEPHONE NUMBER 608-890-2667

Report Title

Final Report: Growth of Large-Area, Free-Standing, Ultrathin 2D Nanomaterials at Solution Interface

ABSTRACT

The development of large and ultrathin nanosheets has been focused on naturally layered materials – the van der Waals solids, such as graphene and transition metal dichalcogenides. Bottom-up synthesis of nanosheets of non-layered materials has been unsatisfactory and limited success has been achieved on nanosheets with sizes below a few hundred nanometers. In this project, We demonstrated that surfactant monolayers could serve as a floating template supporting the nucleation and growth of 2D nanomaterials in large area beyond the limitation of van der Waals solids. Through this approach, 2 to 3 nm thick, monocrystalline ZnO nanosheets with sizes up to tens of microns were synthesized. They are freestanding and densely distributed at the water-air interface without any overlapping. The nanosheets are readily to be transferred onto arbitrary substrates for further device fabrication. Compared with conventional expitaxy where substrate and grown material must match in lattice parameters, ionic layer epitaxy emplys the surfactant monolayer whose packing density adapts to the sub-phase metal ions and guides the epitaxial growth of inorganic nanosheets. Despite the infamous doping asymmetry of ZnO, the nanosheets showed the rare and most coveted p-type conductivity.

Enter List of papers submitted or published that acknowledge ARO support from the start of the project to the date of this printing. List the papers, including journal references, in the following categories:

(a) Papers published in peer-reviewed journals (N/A for none)

Received Paper

TOTAL:

Number of Papers published in peer-reviewed journals:

(b) Papers published in non-peer-reviewed journals (N/A for none)

Received Paper

TOTAL:

Number of Papers published in non peer-reviewed journals:

(c) Presentations

Number of Presentations: 0.00

Non Peer-Reviewed Conference Proceeding publications (other than abstracts):

Received	Paper

TOTAL:

Number of Non Peer-Reviewed Conference Proceeding publications (other than abstracts):

Peer-Reviewed Conference Proceeding publications (other than abstracts):

Received	Paper

TOTAL:

Number of Peer-Reviewed Conference Proceeding publications (other than abstracts):

(d) Manuscripts

Received	Paper	
07/15/2015	1.00	Fei Wang, Jung-Hun Seo, Guangfu Luo, Matthew B. Starr, Zhaodong Li, Dalong Geng, Shaoyang Wang, Dane Morgan, Zhenqiang Ma, Xudong Wang. Nanometer-Thick Single-Crystalline Nanosheets Grown at the Water-Air Interface, Nature (Submitted) (06 2015)

TOTAL: **1**

Number of Manuscripts:

Books

Received Book

TOTAL:

Received Book Chapter

TOTAL:

Patents Submitted

Patents Awarded

Awards

Graduate Students

NAME	PERCENT_SUPPORTED
FTE Equivalent:	
Total Number:	

Names of Post Doctorates

NAME	PERCENT_SUPPORTED
Fei Wang	1.00
FTE Equivalent:	**1.00**
Total Number:	**1**

Names of Faculty Supported

NAME	PERCENT_SUPPORTED	National Academy Member
Xudong Wang	0.05	
FTE Equivalent:	**0.05**	
Total Number:	**1**	

Names of Under Graduate students supported

NAME	PERCENT_SUPPORTED
FTE Equivalent:	
Total Number:	

Student Metrics

This section only applies to graduating undergraduates supported by this agreement in this reporting period

The number of undergraduates funded by this agreement who graduated during this period: 0.00

The number of undergraduates funded by this agreement who graduated during this period with a degree in science, mathematics, engineering, or technology fields:..... 0.00

The number of undergraduates funded by your agreement who graduated during this period and will continue to pursue a graduate or Ph.D. degree in science, mathematics, engineering, or technology fields:..... 0.00

Number of graduating undergraduates who achieved a 3.5 GPA to 4.0 (4.0 max scale):..... 0.00

Number of graduating undergraduates funded by a DoD funded Center of Excellence grant for Education, Research and Engineering:..... 0.00

The number of undergraduates funded by your agreement who graduated during this period and intend to work for the Department of Defense 0.00

The number of undergraduates funded by your agreement who graduated during this period and will receive scholarships or fellowships for further studies in science, mathematics, engineering or technology fields: 0.00

Names of Personnel receiving masters degrees

NAME
Total Number:

Names of personnel receiving PHDs

NAME
Total Number:

Names of other research staff

NAME	PERCENT_SUPPORTED
FTE Equivalent:	
Total Number:	

Sub Contractors (DD882)

Inventions (DD882)

Scientific Progress

See attachment

Technology Transfer

Final Progress Report

Contents

1. Problem studied in this project

In this project, we developed a novel and robust synthesis strategy for ultrathin metal oxide nanosheets from non-layered materials, and we studied the structural and growth mechanism of the nanosheets, as well as the experimental factors that control the thickness of the nanosheets.

Two-dimensional (2D) nanomaterials, particularly when their thickness is just one or a few atomic layers, exhibit physical properties dissimilar to those of their bulk counterparts and other forms of nanostructures. Graphene and transition metal dichalcogenides (TMDs) have epitomized the applications of 2D nanostructures in many electronic, optoelectronic, and electrochemical devices.[1-4] Nonetheless, real-world 2D nanostructures so far have been largely limited to naturally layered materials, i.e. the van der Waals solids, synthesized either from top-down or bottom-up.[5,6] Unlike one-dimensional (1D) nanostructures whose growth mechanisms have been well described, syntheses of ultrathin 2D nanomaterials from non-layer materials without an epitaxial substrate have remained a case-by-case practice. In the sporadic literature reports, such as PbS nanosheets by oriented attachment and palladium nanosheets by a solvothermal method,[7,8] the size of the nanosheets is usually below one micron and much smaller than that of graphene and TMDs, which presents myriad fabrication challenges for real devices. In this regard, a novel and yet robust synthesis strategy dedicated to the growth of general 2D nanostructures of large sizes would enable many novel materials to be grown at a practical dimension for applications.

In this project, we demonstrated that surfactant monolayers could serve as a soft template supporting the nucleation and growth of 2D nanomaterials in large area beyond the limitation of van der Waals solids and demonstrated the properties of the materials grown by this strategy. Specifically, the following proposed problems, have been studied:

1. The synthesis of metal oxide nanosheets that are only a few atomic layers thick and of large single-crystalline grains.
2. The understandings of epitaxial relationship and chemical interactions between the surfactant monolayer and the nanosheets grown underneath.
3. The control over the thickness of the nanosheets.

2. Results

2. 1. Synthesis, structural characterization, and growth mechanism of ZnO nanosheets

In this synthesis, oleylsulfate anionc monolayers were employed to guide the growth of ~1-2 nanometer thick single-crystalline ZnO nanosheets with sizes up to tens of microns at the water-air interface. Sodium oleylsulfate was first dissolved in chloroform and subsequently spread over the surface of an aqueous solution containing precursors that would otherwise produce chunky ZnO nanocrystals.[9] While ZnO nanocrystals still form in the bulk part of the solution, there appeared a single layer of non-overlapping ZnO nanosheets that covered the entire water-air interface. As schematically shown in Fig. 1a, the oleylsulfate anions forms a close-paced monolayer at the water-air interface, under which Zn^{2+} cations are supersaturated and precipitate into nanosheets. Much like graphene, when the nanosheets were transferred onto oxide-coated Si substrates, they became very visible under the optical microscope, and this was very useful for subsequent characterization and device fabrication.23 Figure 1B is an optical microscopy image of ZnO nanosheets on a 100 nm SiO_2-coated Si substrate. These nanosheets were densely packed, and the edges of adjacent nanosheets were mostly aligned. Some nanosheets had small particles at their center. We suspect that these particles were grown in the early stage of the reaction when the supersaturation was extremely high. Figure 1C is a scanning electron microscopy (SEM) image of a single triangular nanosheet with edges longer than 20 μm.

This is the typical morphology of the as-received nanosheets on a Si substrate. A topography atomic force microscopy (AFM) scan revealed the nanosheet was 2.28 nm in thickness and nearly uniform across the entire area (Fig. 1d). The surface roughness was found to be 0.2 nm.

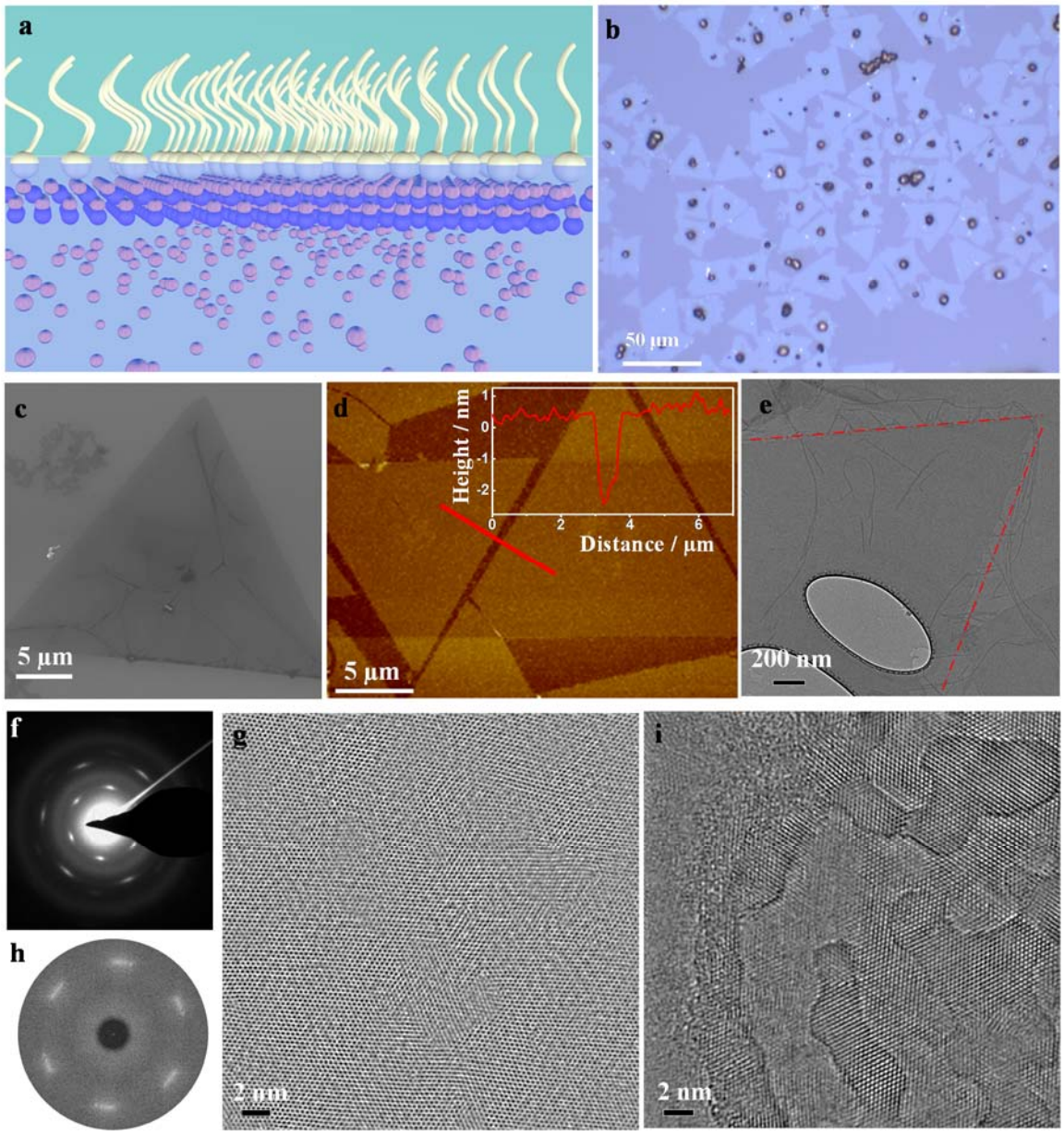

Figure 1 Morphology of ZnO nanosheets. a, Schematic illustration of the formation of ZnO nanosheets directed by surfactant monolayer. **b,** Optical microscopy image of the nanosheets on a silicon substrate coated with 100 nm SiO_2. **c,** SEM image showing a typical nanosheet with an equiangular triangle shape. **d,** AFM topography scans of typical nanosheets with flat surfaces on a Si substrate. **e,** TEM image of a corner of a 20 μm-sized ZnO nanosheet. **f,** Corresponding SAED pattern of the nanosheet shown in E. **g,**

HRTEM image of the same nanosheet. **h,** Corresponding Fourier transformation that shows a hexagonal symmetry. **i,** HRTEM image of a nanosheet showing overlayer growth.

Transmission electron microscopy (TEM) was applied to investigate the crystallinity of these nanosheets as well as their formation mechanism. Figure 1E shows a corner of a triangular nanosheet, which is slightly darker in contrast compared to the background due to its ultra-small thickness. For a clear presentation, we highlighted the edges with red dashed lines. Several very thin whiskers also were observed, which might be concentrated surfactant residues. Selective area electron diffraction (SAED) pattern revealed a single-crystalline hexagonal lattice with a d-spacing of 0.281 nm, which matches the Wurtzite ZnO (0001) facet (Fig. 1f). High-resolution (HR) TEM images were obtained on the area through the holes of the holey-carbon film, as shown in Fig. 1g. The HRTEM revealed the single-crystalline nature of the nanosheet; whereas dislocations or small defective areas could also be observed on the nanosheet. Corresponding fast Fourier transfer (FFT) pattern of the HRTEM image clearly matches the SAED pattern, confirming the single crystallinity across the entire nanosheet (Fig. 1h). Nanosheets with uneven surfaces were also observed as shown in Fig. 1i. There appear to be a developing overlayer on the nanosheet surface, indicative of a layer-by-layer growth mode.

The nanosheets at the water-air interface were collected at different reaction times to investigate their formation mechanism. TEM images in Figs. 2A-D and the conceptual drawing below them respectively illustrate the crystal structure evolution of the nanosheets. What appeared at the interface first was a continuous amorphous film (Fig. 2a), which is supported by the inset FFT pattern. Tiny crystallites are embedded in the largely amorphous film although hardly visible. These crystallites then grew in lateral size, and were all oriented with the same hexagonal crystal plane exposed; however, their in-plane rotation appeared to be stochastic, as shown in Fig. 2b. The inset FFT pattern confirmed such a textured structure, with a single ring

that matches the d-spacing of the SAED pattern. As the crystallites grew larger, they merged at an aligned orientation into a contiguous, single-crystalline network coexisting with much reduced amorphous region confined between the nanosheets (Fig. 2c). A single set of 6-fold symmetric spots appeared in the FFT pattern of the TEM image. Eventually, the amorphous area was fully crystallized and the nanosheet became single-crystalline with few dislocations that were likely formed by the mis-orientation of merged crystalline areas during the formation process (Fig. 2d).

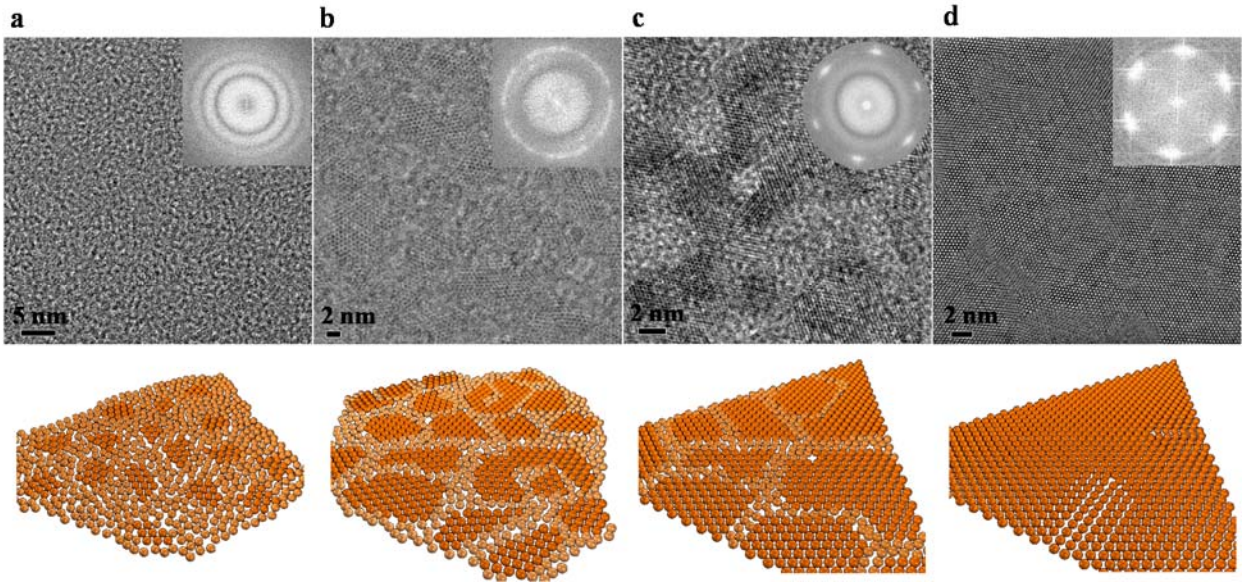

Figure 2. TEM images and schematic drawings showing the time-dependent evolution of ZnO nanosheets. a, Mostly amorphous films with tiny crystalline grains and curved edges. **b,** More crystalized nanosheets with 2 to 3 nm grains that are randomly oriented. **c,** These crystalized grains grew bigger and had aligned orientation. **d,** Large-area single-crystalline nanosheet. The insets are fast Fourier transfer patterns of the TEM images, respectively. The four schematic drawings below TEM images conceptually depict the crystal structure of each stage during the evolution of ZnO nanosheets. Regions with lighter gold colored spheres are amorphous and regions with deeper gold colored spheres are crystalized.

2. 2. The epitaxial relationship and chemical interactions between the surfactant monolayer and the nanosheets grown underneath.

Our studies showed that the highly ordered, densely packed anionic monolayer of oleylsulfates at the water-air interface has not only stimulated the growth of large, amorphous ZnO films but has also directed the crystallization process of ZnO nanosheets across a large 2D scale. This multistep process began when the anionic monolayer created a negative surface potential that raised the concentration of Zn^{2+} near the monolayer, resulting in the initial formation of the amorphous films described in Fig. 2a. As the amorphous ZnO film began to crystallize, the long range order of the oleylsulfate monolayer coordinated the orientation between independent ZnO crystallites owing to the strong association between the oleylsulfate molecules and the Zn^{2+} ions below. To test this hypothesis, control experiments were conducted using stearic acid in place of oleylsulfate, as it has a similar molecular structure but a different headgroup (carboxylate). Millimeter-sized, nanocrystal-percolated amorphous films without faceted edges were obtained, very similar to the initial amorphous films when oleylsulfate was used. No single-crystalline nanosheets triangles were observed after extended reaction time. This corroborated our argument that specific bonding between sulfate groups and ZnO surface are needed for the crystallization of ZnO nanosheets. It is also important to note that large, single crystalline nanosheets were obtained with great reproducibility without controlling the surface pressure of the monolayer. This fact suggests that the epitaxial relationship between the Zn^{2+} ions and the ionic surfactant monolayer is very robust and can tolerate small variations in the intermolecular spacing in the monolayer. We believe this is because the Zn^{2+} ions imposed a profound influence on the arrangement of the ionic surfactant monolayer, as metal ions in the aqueous sub-phase, especially multivalent ones, can affect the 2D arrangement of surfactant

molecules in monolayers and improve their stability *via* electrostatic and coordination interactions. Therefore, during the formation of ZnO nanosheets, the oleylsulfate anions can spontaneously and simultaneously adapt to the ZnO lattice. This growth therefore occurs through a two-way epitaxy process, and is thus named as *adaptive ionic layer epitaxy* (AILE).

2. 3. An electric double layer model on the thickness of nanosheets grownby AILE

In order to understand the chemical environment for the formation of ZnO nanosheets, we simulated the effects of a negatively charged surfactant monolayer on the concentration profile of Zn^{2+}. We assumed the average area occupied by a single oleylsulfate molecule in the monolayer is 0.2 nm^2, which corresponded to a charge density of -0.801 C m^{-2}. A positively charged stern layer with a uniform charge density of 0.736 C m^{-2} was established at a distance of 0.3 nm away from the surfactant layer. The electric field resultant from superimposing both charged surfactants and Stern layers influences the charged species in solution, attracting (concentrating) or repulsing (diluting) positive and negative charged ions, respectively. The electrical potential profile, (φ(x)), between the Stern layer and bulk solution was solved numerically using the following expression:

$$\left(\frac{d\phi}{dx}\right)^2 = \frac{2\mathrm{kT}}{\epsilon\epsilon_0}\sum_i \left(\mathrm{n_i^0}\left[\mathrm{e}^{\left(\frac{-\mathrm{z_i e}\phi}{\mathrm{kT}}\right)} - 1\right]\right) \qquad (1)$$

where φ is the potential relative to bulk solution, x is a measure of distance into solution and perpendicular to the monolayer surface, k is the Boltzmann constant, T is absolute temperature, $\mathrm{n_i^0}$ is the bulk concentration of ion i, z_i is the charge of ion i, and e is the charge of an electron.[10] The potential adjacent to the Stern layer at the closest approach by ions in solution, φ(6Å), was taken as 0.065 V. As the concentrations of all species are constantly changing during the reaction, we only calculated the chemical environment near the interface at the relevant

reaction time (1.5 hours into the reaction) assuming the concentration of each ion as listed in Table S1. Consistent with Eq. (1), the ratio of concentrations of species *i* in bulk solution (n_i^0) at bulk solution potential ($\varphi^0 = 0$) to its concentration (n_i) found at any other potential (φ) is given by:

$$n_i = n_i^0 e^{\left(\frac{-z_i e \phi(x)}{kT}\right)} \quad (2)$$

In the case of Zn^{2+}, n_i^0 is 18.72 mM, and z_i is 2. Figure 3 is a plot of Zn^{2+} concentration as a function of distance from the surfactant monolayer into the bulk solution. It can be observed that the concentration of Zn^{2+} ions dropped drastically within a very short distance from the Stern layer. At distant x = 1.5 nm, its concentration became only marginally different from bulk concentration. Therefore, the Stern layer and the diffuse Gouy layer up to 1.5 nm from the interface constituted a Zn^{2+}-concentrated zone. In Fig. 3 we also marked the measured thickness of the single-crystalline nanosheets and the amorphous films by black squares and red round dots, respectively. The single-crystalline triangular ZnO nanosheets and amorphous films have an average thickness of 2.73±0.33 nm and 3.28±0.41 nm, respectively. The single-crystalline ZnO nanosheets were generally thinner than the amorphous films, possibly due to a volume reduction and removal of non-native ions (*e.g.* nitrate and ammonium ions) during the crystallization. Given the fact that the oleylsulfate adsorbed on the surface of nanosheets may have contributed a thickness of ~2 nm,[11] the thickness of the amourphous ZnO nanosheets is about the same as the width of the Zn^{2+}-concentrated zone near the interface (~1.5 nm). We therefore propose that this Zn^{2+}-concentrated zone has provided an interfacial chemical environment different from the bulk concentration which drove the growth of ZnO nanosheets and has determined the thickness of the initial amorphous ZnO films that subsequently transformed into single-crystalline nanosheets.

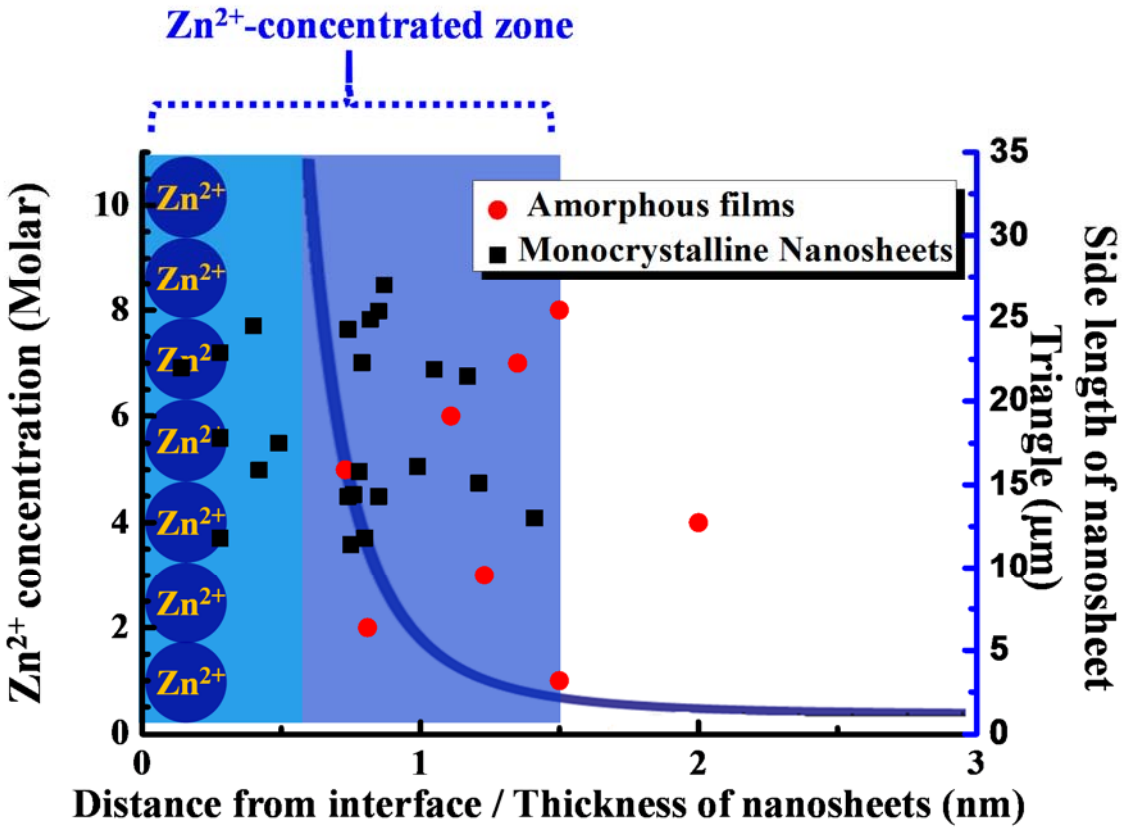

Figure 3. Calculation of the Zn^{2+} concentration profile and its relation with the thickness of ZnO nanosheets. The light blue shaded band represents a positively charged stern layer primarily composed of Zn^{2+} ions. The blue curve plots the concentration of Zn^{2+} from the end of the Stern layer (blue shaded area within the first 0.6 nm) into the bulk solution. The black squares and red round dots marks the thickness of single-crystalline nanosheets and amorphous films formed prior, respectively, measured by AFM. The right vertical axis is the side length of single-crystalline nanosheet triangles. Note that the sizes of amorphous films are hundreds of microns and are not displayed in this plot.

2. 4. Electrical properties of ZnO nanosheets

As exotic physical properties can arise when the thickness of a material is reduced to a single or a few atomic layers, the electronic property of ZnO nanosheets were investigated by fabricating thin film transistors (TFTs) with a back gate configuration (inset of Fig. 4a). The I_d-V_g curve shows an increasing source-drain current (I_d) as the gate voltage (V_g) scans from positive to negative (Fig. 4a). This is a typical *p*-type semiconductor behavior. The I_d-V_d curves

at different gate voltages shown in Fig. 4b further confirmed the *p*-type conductivity of the ZnO nanosheets. Higher positive drain current was obtained as the gate voltage went more negative. Based on the dimension of the nanosheets and the transconductance derived from Fig. 4a, the carrier concentration and hole mobility of the nanosheets were estimated to be 1.4×10^{18} cm^{-3} and 0.01 cm^2/Vs, respectively (Supplementary Information S1). We fabricated and measured 20 devices and carrier concentration and hole mobility values were all within the same order of magnitude.

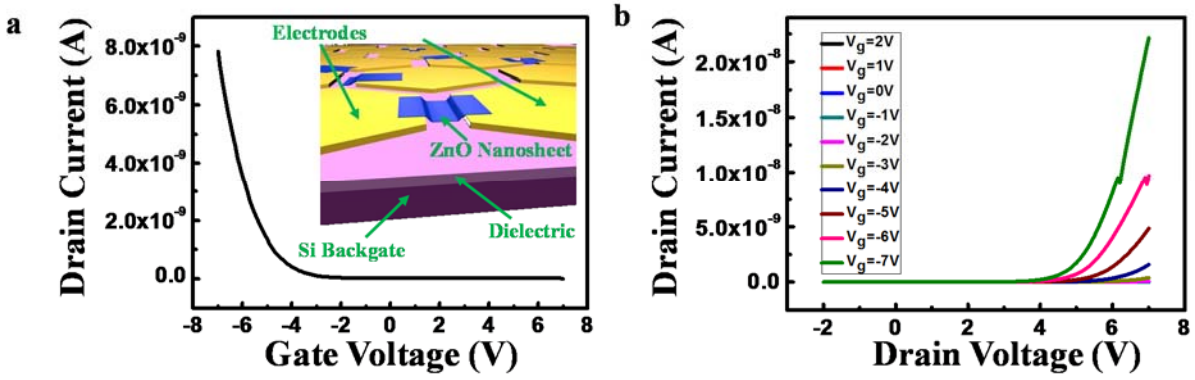

Figure 4. Electronic properties of ZnO nanosheets. a, Drain current *versus* gate voltage when the drain voltage was 5V. The gate voltage scan was from 7V to -7V. Inset is the schematic of nanosheet-based TFTs. **b,** Drain current *versus* drain voltage at different gate voltages from 2V to -7V with a 1V step.

References

1 Matte, H. S. S. R. *et al.* MoS_2 and WS_2 Analogues of Graphene. *Angew. Chem., Int. Ed.* **49**, 4059-4062 (2010).

2 Rao, C. N. R., Sood, A. K., Subrahmanyam, K. S. & Govindaraj, A. Graphene: The New Two-Dimensional Nanomaterial. *Angew. Chem., Int. Ed.* **48**, 7752-7777 (2009).

3 Lei, W. W., Portehault, D., Liu, D., Qin, S. & Chen, Y. Porous boron nitride nanosheets for effective water cleaning. *Nat. Commun.* **4** (2013).

4 Lukowski, M. A. *et al.* Enhanced Hydrogen Evolution Catalysis from Chemically Exfoliated Metallic MoS_2 Nanosheets. *J. Am. Chem. Soc.* **135**, 10274-10277 (2013).

5 Zhang, Y., Zhang, L. Y. & Zhou, C. W. Review of Chemical Vapor Deposition of Graphene and Related Applications. *Acc. Chem. Res.* **46**, 2329-2339 (2013).

6 Lee, Y. H. *et al.* Synthesis of Large-Area MoS_2 Atomic Layers with Chemical Vapor Deposition. *Adv. Mat.* **24**, 2320-2325 (2012).

7 Schliehe, C. *et al.* Ultrathin PbS Sheets by Two-Dimensional Oriented Attachment. *Science* **329**, 550-553 (2010).

8 Huang, X. Q. *et al.* Freestanding palladium nanosheets with plasmonic and catalytic properties. *Nat. Nanotechnol.* **6**, 28-32 (2011).

9 Wang, F. *et al.* Nanometer-Thick Single-Crystalline Nanosheets Grown at the Water-Air Interface. In peer review (2015).

10 Bard, A. J. & Faulkner, L. R. *Electrochemical Methods: Fundamentals and Applications*. (Wiley, 2000).

11 Xu, T., Morris, T. A., Szulczewski, G. J., Metzger, R. M. & Szablewski, M. Current-voltage characteristics of an LB monolayer of didecylammonium tricyanoquinodimethanide measured between macroscopic gold electrodes. *J. Mater. Chem.* **12**, 3167-3171 (2002).